water

MDPI

Article

Optimized Artificial Neural Networks-Based Methods for Statistical Downscaling of Gridded Precipitation Data

Amir Hossein Salimi [1], Jafar Masoompour Samakosh [2], Ehsan Sharifi [3,4,*], Mohammad Reza Hassanvand [1], Amir Noori [5] and Hary von Rautenkranz [6]

1 Department of Water Engineering and Hydraulic Structure, Semnan University, Semnan 35131, Iran
2 Department of Geography, Razi University, Kermanshah 67146, Iran
3 Department of Meteorology and Geophysics, University of Vienna, Vienna 1090, Austria
4 Institute of Meteorology and Climatology, University of Natural Resources and Life Sciences (BOKU), Vienna 1180, Austria
5 Department of Water Resource Management, Razi University, Kermanshah 67146, Iran
6 Department of Environmental Geosciences, University of Vienna, Vienna 1090, Austria
* Correspondence: ehsan.sharifi@univie.ac.at; Tel.: +43-676-976-6304

Received: 23 June 2019; Accepted: 8 August 2019; Published: 10 August 2019

Abstract: Precipitation as a key parameter in hydrometeorology and other water-related applications always needs precise methods for assessing and predicting precipitation data. In this study, an effort has been conducted to downscale and evaluate a satellite precipitation estimation (SPE) product using artificial neural networks (ANN), and to impose a residual correction method for five separate daily heavy precipitation events localized over northeast Austria. For the ANN model, a precipitation variable was the chosen output and the inputs were temperature, MODIS cloud optical, and microphysical variables. The particle swarm optimization (PSO), imperialist competitive algorithm,(ICA), and genetic algorithm (GA) were utilized to improve the performance of ANN. Moreover, to examine the efficiency of the networks, the downscaled product was evaluated using 54 rain gauges at a daily timescale. In addition, sensitivity analysis was conducted to obtain the most and least influential input parameters. Among the optimized algorithms for network training used in this study, the performance of the ICA slightly outperformed other algorithms. The best-recorded performance for ICA was on 17 April 2015 with root mean square error (RMSE) = 5.26 mm, mean absolute error (MAE) = 6.06 mm, R^2 = 0.67, bias = 0.07 mm. The results showed that the prediction of precipitation was more sensitive to cloud optical thickness (COT). Moreover, the accuracy of the final downscaled satellite precipitation was improved significantly through residual correction algorithms.

Keywords: optimize artificial neural networks; downscaling; satellite precipitation monitoring; cloud optical and microphysical properties

1. Introduction

Whereas climatic parameters such as temperature and pressure are nowadays well documented by in situ and remotely sensed platforms, and well predicted by numerical weather prediction models, precipitation, as one of the key variables in hydrometeorological applications, is still lacking sufficient monitoring precision, since it is characterized by high variability in space and time. Even in the densely populated parts of the midlatitudes, in situ precipitation networks are not sufficient to catch every small-scale event. Moreover, the lack of complete coverage with weather radar systems and their uncertainties does not allow filling the spatial gaps.

As precipitation varies greatly in space and time, gridded precipitation data in high spatiotemporal resolution is a considerable requirement as input for hydrometeorological and water resources management applications. This type of data is highly important for timely action (e.g., the initiation of landslide and mudslide movement) and decision making, such as evacuating an area with high potential for flooding, or to secure food and water supply [1]. However, high spatiotemporal resolution datasets are usually available only on a country level or cover a specific geographical region. These type of datasets might be obtained by interpolation of in situ observations and reanalysis products, or derived through remote sensing observations [2].

The monitoring of precipitation from space opens a new era of precipitation observation. Hence, precipitation and hydrologic cycle studies are a hot topic in atmospheric science. High-resolution satellite precipitation estimates (SPEs) provide an effective global source of uninterrupted data for various water-related applications, especially over regions where ground-based observations are often lacking or sparse. These factors are underlying reasons why the increasing use of satellite data, which provide much better geographical coverage despite the potential limited accuracy, depends on precipitation products. The limited accuracy could be caused by various reasons e.g., algorithm, orographic effects, cloudy and/or snowy conditions, the relatively short observation periods, and type of sensors [3].

Satellite products, as well as all other types of datasets, are subject to errors and uncertainties. Therefore, these data should be evaluated before being applied in climatological and hydrometeorological applications. Comparing a pixel of satellite-based precipitation with one rain-gauge may not give reliable results because satellites show the average of precipitation over an area (a pixel), while rain-gauges show the amount of precipitation a few square meters around the gauge, this producing the point-area effect. This may be significant in highly variable events, whereas precipitation within a region may occur in smaller scales than the pixel size of satellites. Downscaling may address such a limitation. When data are needed for small basin applications such as hydrological studies, the spatial resolution and accuracy of land-atmosphere variables, e.g., precipitation, becomes very important [4]. During the last decade, many regional- or global-scale studies have evaluated the accuracy of different SPE products to obtain insight into the merit of different products and their innovations [5–8]. For instance, Sharifi et al. [9] evaluated IMERG-V03 (Integrated Multi-satellite Retrievals for GPM; Global Precipitation Measurement), 3B42-V7 (Tropical Rainfall Measuring Mission), and ERA-Interim [10–12] against meteorological stations over the different climate conditions in Iran. They characterized higher correlation in monthly and seasonal time scales, while the results indicated lower correlation in a daily time scale. Their results indicated IMERG underestimates precipitation slightly and outperforms other products in all regions. In another study, they examined the newer version of IMERG-V04 final-run (FR) and real-time (RT) for the occurrence and statistical characteristics of precipitation intensity in daily and hourly time-scales. They found that IMERG-V04 indicated better results in a daily time scale while for hourly precipitation estimation there was larger negative total bias [13]. Compared to previous studies, further maturity of SPE products can be expected including improvement in constellation and multisensory data fusion, and in sensor-specific retrieval algorithms that recognize, and account for, observed spatial structures [14,15].

Precipitation estimate uncertainties propagate through related modeling predictions. Consequently, increasing the accuracy by downscaling and bias correction procedures is critical for hydrologists and meteorologists to produce local-scale information so that it can be employed in decision-making activities [16]. Spatial downscaling is the means of establishing a mathematical relationship between the large-scale atmospheric predictor variables to local- or station-scale meteorological records. Among the variety of downscaling techniques in the literature, the two major methods can be identified as dynamic and statistical downscaling. However, among the wide range of statistical downscaling techniques which have been developed over the last decade, each method generally belongs to one of the following categories: Regression (transfer function), stochastic weather generators, and weather typing schemes [17]. The artificial neural network (ANN) is one of the methods that have been implemented to derive the relationships between the predictor and predictand. Using ANN algorithms has been proven to have accessible results, especially to model the relationship among nonlinear parameters [18]. For example, Hassanvand et al. [19] applied different meta-algorithms such as particle swarm optimization (PSO), imperialist competitive algorithm (ICA), genetic algorithm(GA) and BAT, as well as a combination of these algorithms with ANN and adaptive network-based fuzzy inference system (ANFIS) algorithms for flood routing to estimate the flood volume. During the last decade, optimization algorithms have been an active area of research. As problems become more complex, better optimization algorithms were needed. Many populations-based algorithms were proposed for solving unconstrained optimization problems.

Although gradient descent is the most popular optimization algorithm, metaheuristics have been established as one of the most practical approaches to simulation optimization. GA, PSO, and BAT algorithms are the most popular optimization algorithms which employ a population of individuals to solve the problem on hand. Khan et al. [20] compared gradient descent and heuristic algorithms. They indicated the advantages of the BAT algorithm over the other algorithms in the context of eLearning. Another study showed that by using a simple genetic algorithm (GA) it is possible to optimize ANNs, and concluded that GAs are a competitive alternative to gradient-based methods [21].

In an effort to obtain more reliable precipitation from SPE, Sharifi et al. [22] recently downscaled the IMERG-FR V05B product through multiple linear regression (MLR), ANN, and spline interpolation, deriving a meaningful spatial resolution for hydrometeorology and water resource studies. Since a bilateral relationship should exist between clouds and precipitation [23], they adapted high-resolution cloud optical and microphysical properties with the spatial resolution of 1 km, derived from the moderate resolution imaging spectroradiometer (MODIS) sensor [24], as the auxiliary data (predictor variables) for downscaling of SPE at daily time-scale to emphasize on heavy precipitation. To obtain downscaled daily precipitation product over northeast Austria, they utilized cloud optical thickness (COT), cloud effective radius (CER), and cloud water path (CWP). They significantly improved the accuracy of IMERG resolution, but some weak points were evident when using simple ANN and using only MODIS cloud properties data. The spline interpolation technique slightly outperformed other models in their study. Although altitudes did not significantly affect precipitation patterns, the interpolation provided by the spline method in complex terrain needs further evaluation. Systematic anomalies for the spatial distribution of precipitation obtained by the ANN downscaling method were found in the study. Some values were clearly greater than neighboring pixels and included more variations in the precipitation amount and errors compared with neighboring pixels. There was a gradual trend of no anomalies for continuous spatial variations when considering MLR-based downscaled data along with spline interpolation. This indicates that it was probably the ANN model failing to provide the correct location in high-intensity precipitation [22,25]. These issues motivated us to further study this limitation and improve the neural networks techniques for precipitation downscaling, particularly for extreme precipitation events.

Although there are numerous important issues to address in SPEs e.g., light rainfall, complex precipitation systems, cold- and warm-season precipitation, precipitation at high latitudes, and tropical areas; our focus is on heavy precipitation ($p > 30$ mm/day) events, which are characterized by high space–time variability and, as a consequence, might pose an additional challenge due to rather coarse IMERG pixels ($0.1° \times 0.1°$). In this context, the challenge is to define the spatial scale at which SPE must be produced with higher accuracy to be more useful in hydrometeorological applications at finer spatial scales (1 km). Therefore, this study aimed to optimize the methodology of Sharifi et al. [22], using different algorithms, e.g., PSO, ICA, and GA. Moreover, in this study alongside the CER, CWP, and COT from MODIS sensor, temperatures from ERA5, the newest product released by the Copernicus Climate Change Service (C3S) [26] for northeast Austria were used. Further, in this research, the possibilities of using optimized ANN techniques, fine resolution of cloud, and temperature products for downscaling IMERG were evaluated.

2. Data and Methods

2.1. Data

To examine the improvement of our downscaling methods in comparison with the previous study by Sharifi et al. [22], the Northeast part of Austria was selected. The selected region (black box) is located at the easternmost extension of the Alps and, according to the Köppen-Geiger classification updated by Rubel et al. (2017) (see Figure 1), falls into the Cfb classification of a warm temperate zone with less than 600 mm in annual precipitation [27]. The altitude of the region (black box) is moderate and does not have a significant effect on precipitation systems. The highest area is located in the Southwestern part of the domain, with elevation of approximately 1000–1500 m, and the other parts of the domain have an altitude of approximately less than 1000 m. Both convective and stratiform precipitation types occur over the region.

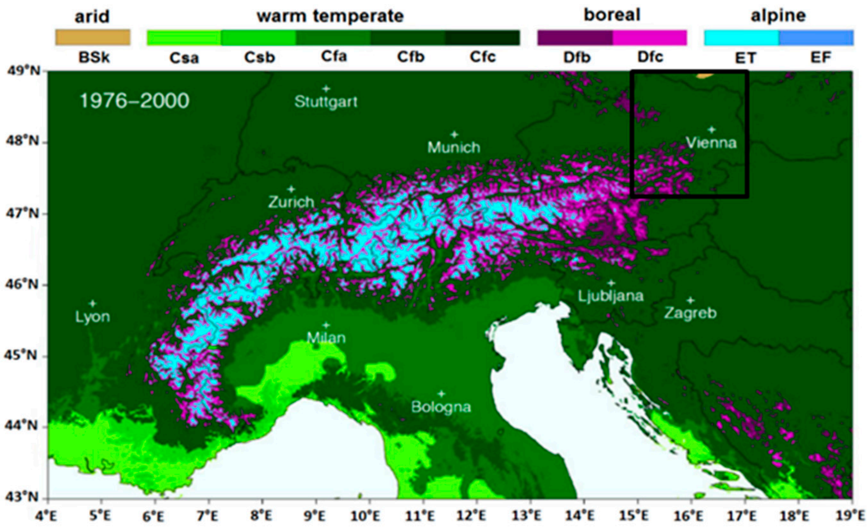

Figure 1. Climate of Austria based on Köppen climate classification—updated by Rubel et al. 2017. The black box indicates the study area.

In this study, in situ precipitation data from the 54 operating synoptic stations with 10 minute intervals, provided by the Zentralanstalt für Meteorologie und Geodynamik (ZAMG)-Austria, were used across the study area. Five precipitation events with equal or higher than 30 mm/day rain intensity were chosen to verify the improvements of the proposed machine learning-based downscaling techniques. These events occurred on 17 April, 23 May, 3 September, 25 September, and 7 October 2015 over the study area.

The Precipitation Processing System (PPS) at NASA's Goddard Space Flight Center released IMERG-V05B data to the public in late November 2017. The dataset includes precipitation since March 2014, but the developers have promised in the retrospective GPM reprocessing, IMERG will incorporate the Tropical Rainfall Measuring Mission (TRMM) data as a calibrator, enabling a start date of January 1998. The datasets from NASA Goddard Earth Sciences Data and Information Services Center (GES DISC) website (https://disc.gsfc.nasa.gov/SSW) are freely accessible to users. In this study, IMERG-FR product used was derived from the various passive microwave (PMW) and infra-red (IR) sensors, gridded, inter-calibrated, and finally, used the monthly precipitation rain-gauges from the Global Precipitation Climatology Centre (GPCC) with the aim of bias correction, and assembled into half-hourly $0.1° \times 0.1°$ fields [10]. The IMERG product covers the selected domain with about 290 $0.1° \times 0.1°$ pixels.

One of the key instruments operating on Terra and Aqua satellites is the moderate resolution imaging spectroradiometer (MODIS). This instrument can provide different variables and describe various features of the land, oceans, and the atmosphere, and the distribution and frequency of cloud cover. This instrument (MYD06 and MOD06 for Aqua and Terra MODIS, respectively) measures both physical and optical cloud properties with spatial resolutions of 1 km, using a combination of infrared and visible techniques [28].

MYD06 was launched aboard Terra (1999), which passes the equator from north to south during mornings and MOD06 was launched on Aqua (2002), passing the equator south to north during afternoons. The MODIS sensors can monitor the entire Earth's surface through both satellites over a period of one to two days, deriving data from 36 wavelength spectral bands ranging from 0.4 to 14.4 μm. The design aim was to increase the accuracy of cloud imaging via the twin MODIS, by reducing optical effect shadows and glares during the mornings and afternoons. The data can be freely accessed from the Level 1 and Atmosphere Archive and Distribution System (LAADS) Distributed Active Archive Center (DAAC) website (https://ladsweb.modaps.eosdis.nasa.gov).

ERA5 data are produced using four-dimensional variable (4D-Var) data assimilation in the Integrated Forecast System (IFS) of the European Centre for Medium-Range Weather Forecasts (ECMWF) with vertical, multi pressure (model) levels. There is also the availability of data from the surface or single level that contains example 2D parameters i.e., 2 m temperature. At 06 and 18 UTC there is a provision of two daily forecasts (short, 18 h), and analyses from subdaily and monthly available data. The majority of parameters analyzed, i.e., 2 m temperature, are available from forecasts, as well. The ERA5 high-resolution atmospheric data have a resolution of 0.28125 degrees (31 km), but when downloading the data there is the possibility to resample the data to a higher spatial resolution. This will be done for continuous parameters (e.g., temperature) by default through bilinear resampling methods [26]. Therefore, for consistency to IMERG data, we used the temperature data with 0.1 degree spatial resolution. The data are freely accessible to users from Climate Data Store (CDS) website (https://cds.climate.copernicus.eu). Table 1 indicates the characteristics of data sets used in this study.

Table 1. Characteristics of data used in this study.

	Temporal Resolution	Spatial Resolution	Spatial Coverage	Parameter
IMERG	30 min	0.1°	60° N-S	Precipitation
MODIS	1–2 images daily	1 km	90° N-S	CER, CWP, and COT
ERA5	Hourly	0.1°	90° N-S	Temperature

2.2. *Methodology*

During the last years, ANNs have been widely used in various fields of science, engineering, etc. Recently, using the ANN has been brought into consideration for downscaling of satellite data. Generally, the ANN models have performed well in different terrestrial terrain and climate regions by using various combinations of predictors (auxiliary data). According to Sharifi et al. [22], who concluded that ANN can predict precipitation with cloud optical and microphysical properties data input, this study focuses on optimizing the ANN by comparing different optimization algorithms.

In this study, we assumed that the statistical relationship among the CER, CWP, COT, and temperature as predictive variables (inputs), and that IMERG precipitation data at a coarse scale (0.1°), would be preserved at a finer scale (1 km), providing additional detail in local precipitation fields. In other words, the rationale underlying this approach is that the spatial pattern of precipitation can be related to other covariates (e.g., cloud optical and microphysical variables, temperature, altitude) that have higher spatial resolution. Then, the precipitation spatial resolution can be improved by constructing a functional relationship between precipitation and these factors. Then, by using the high-resolution factors as input data, implementing the ANN to predict the target precipitation trend. However, since the model cannot well explain the actual spatial variability of precipitation at fine-scale, the residual correction technique at coarse scale is also utilized (i.e., interpolated to fine-scale and added up to the predicted precipitation at fine-scale), which produces the final downscaled precipitation. This method has been used in various studies [22,25,29–32].

Hence, first of all, the cloud variables were remapped using the bilinear method in order to match the cloud variables to the IMERG, native grid size and the regression relationship between the predictive variables and the 0.1° IMERG precipitation data were obtained.

2.2.1. Artificial Neural Network (ANN)

ANN imitates modelling of the human brain's neural network via uses of nonlinear patterns [33] for complex system modelling. Although ANN is not totally comparable to natural neuronal systems, ANN makes important contributions to some applications such as pattern separation, linear, or non-linear mapping [34].

The structure of ANN is built on relationships between nodes that determine communicational weights and functional activity. ANN's structure typically has input, middle/hidden, and output layers. The input layer transmits the data and the output layer holds estimated values from the network. The middle or hidden layers are composed of processor nodes and process data. The number of hidden layers and the number of their respective nodes are determined by the trial and error method. Inputs and desired outputs are needed for supervised learning. Processing of inputs and comparison of resulting outputs against desired outputs is done by the network. Errors are propagated back through the network, triggering the system to modify the weights of the network. This process is repeated with continuous adjustments. For the effective use of ANN, it is essential that the model is trained and tested, with proper selection and preprocessing steps, as well as proper network architecture [35].

The structure of the ANN model used is:

(a) 70%, 15%, and 15% of the data used for training, verification, and test of the data, respectively.
(b) One hidden layer.
(c) Type of the network: Feed-Forward ANN.
(d) Training function: TRAINLM (Levenberg-Marquardt training algorithm).

2.2.2. Imperialist Competitive Algorithm (ICA)

ICA, introduced by Atashpaz and Lucas [36], is inspired by the sociopolitical development of imperialism within human societies. Through the mathematical modeling of this historical phenomenon, they proposed a powerful optimization algorithm.

Within a search space, there is a randomized generation of countries and a designation of being imperialist is given to many of the most powerful countries. The imperialist countries are randomly assigned weaker countries known as colonies. The number of imperialist countries is dependent on its power. Language and culture are tools of the imperialist countries to assimilate colonies within the algorithm. Modelling of this assimilation is achieved through the colonies moving randomly in the direction of their imperialist country within the search space. As the algorithm moves countries, a colony may accumulate more power than its imperialist colonizer. When this happens, the colony and colonizer country will be replaced. There is competition between the imperialist countries during each repetition. This has the weakest colony separate from the weakest imperialist, thus joining a different imperialist country randomly. The probability of the separated colony being assigned is proportional to the power of each imperialist country. If the loss of all colonies occurs for an imperialist country, it is taken over by another more powerful imperialist country. The algorithm runs until there is only one imperialist country remaining. [19,37]. Figure 2 indicates the flowchart of the ICA.

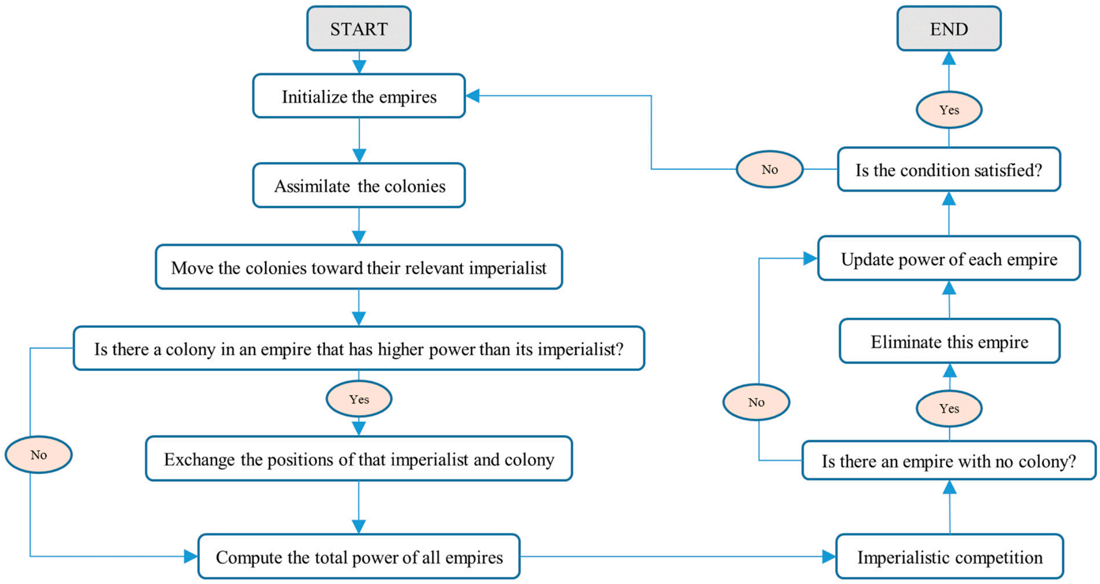

Figure 2. Flowchart of the imperialist competitive algorithm (ICA).

2.2.3. Genetic Algorithm (GA)

Nature has always been the best teacher of humans, and inspired by nature, humans have come up with tools and techniques that are best suited to their life. A genetic or inherited algorithm (GA) is one of these techniques. GA is a numerical optimization method based on Darwin's theory of natural evolution, where the fittest individuals are selected for reproduction. This method has been used in many applications according to its high abilities. Hence, GA is able to solve a wide range of issues, such as the optimal design of frames and hydraulic structures. However, according to previous studies, the GA has proven its ability in real world scenarios to search and solve optimization problems [38,39]. GA starts the search operations from multiple points (chromosomes) in the response surface, each of these points being an initial scheme. The multiple concurrent search points, or a set of chromosomes, is a population. A generation is obtained according to each iterative step and produces a new population [40]. Initial population production can be done completely random or by applying the user's opinion. After creating the initial population, the chromosomes, which are in fact the initial plan, are examined and, according to their fitness, values are assigned. So, as the plan is more compatible and fit with our requirements, more numerical values are assigned. After examination of the fitness of all people in the community, the GA selects the best ones. The selected individuals are subjected to random actions such as selection, mutation, etc., to produce the next generation with fitter parents, and subsequently, a better chance at surviving. Through an interactive process, a generation with the fittest individuals will be found [41]. Figure 3 indicates the flowchart of the GA.

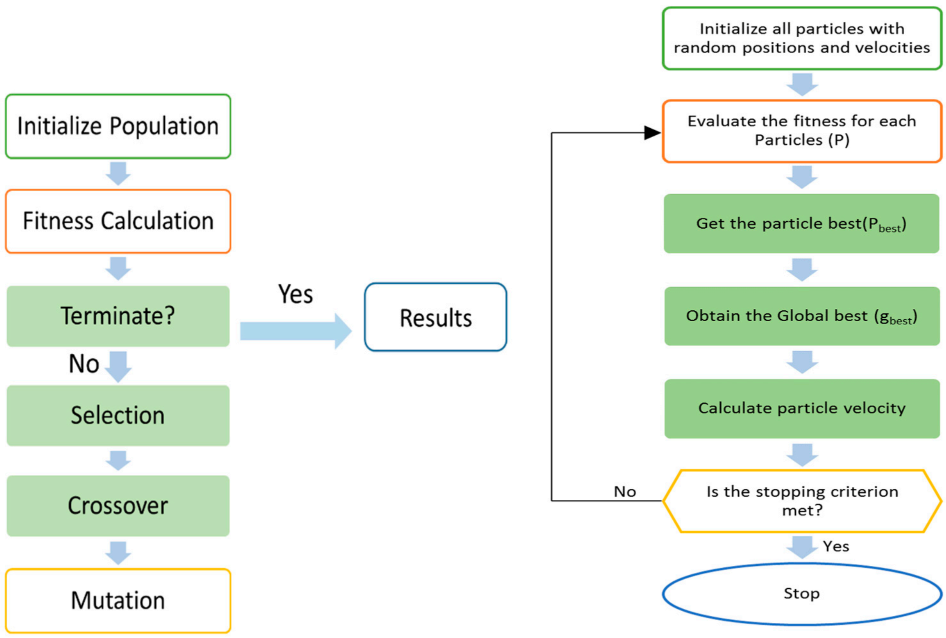

Figure 3. Flowchart of the genetic algorithm (left) and the particle swarm optimization algorithm (right).

2.2.4. Particle Swarm Optimization (PSO) Algorithm

The PSO algorithm proposed by Kennedy and Eberhart [42] for the optimization of continuous nonlinear functions, has been successfully applied across various fields. Inspired by the exchange of information between flying birds and fish movements, PSO is an evolutionary computation technique. Each solution is only a particle in a search space, which has a specific fitness as measured by a fitness function, and each particle has a position in an n-dimensional spatial of the problem calculated in any *tth* repetition (Equation (1)). The particle's velocity is shown by a vector in t^{th} repetition (Equation (2)). The particle stores its former best position in each repetition as a P vector (Equation (3)).

$$X_i^t = \left(x_{i1}^t,\ x_{i2}^t, \ldots,\ x_{in}^t \right) \tag{1}$$

$$V_i^t = \left(v_{i1}^t,\ v_{i2}^t, \ldots,\ v_{in}^t \right) \tag{2}$$

$$P_i^t = \left(p_{i1}^t, p_{i2}^t, p_{in}^t \right) \tag{3}$$

A particle is updated by considering first, the best solution the particle has experienced (best P) and second, following the PSO algorithm, the best position that has been obtained in the population thus far (the best position of g). The position and velocity of each particle are updated with these two values by Equations (4) and (5).

$$V_i(t+1) = WV_i(t) + C_1 r_{1,i}(t)(p_i(t) - X_i(t)) + C_2 r_{2,i}(t)\left(p_g(t) - X_i(t)\right) \tag{4}$$

$$X_i(t+1) = X_i(t) + V_i(t+1) \tag{5}$$

In the above equations, t indicates the number of repetitions. C_1 and C_2 are learning factors. Generally, $C_1 = C_2 = 2$, and controls the amount of a particle displacement in a repetition. r_1 and r_2 are two steady random numbers in [0,1] intervals. W indicates the inertial weight and holds the initial value in the [0,1] interval. In the PSO algorithm, the population gets the initial value by random solutions and the population fitness is calculated iteratively until obtaining the P_{best} and g_{best} values, velocity, and position are updated, respectively. At least, the g_{best} and its fitness are indicated as the output. The final outcome is achieved when the maximum number of generations or a specific value of fitness in g_{best} is reached [36]. Figure 3 indicates the flowchart of the PSO.

To examine and evaluate the performance of models, the R-squared (R^2) coefficient, root mean square error (RMSE), bias, and mean absolute error (MAE) indices were used.

$$R^2 = \left[\sum_{i=1}^{n} (x_i - \overline{x})(y_i - \overline{y}) / \sqrt{\sum_{i=1}^{n} (x_i - \overline{x})^2 \sum_{i=1}^{n} (y_i - \overline{y})^2} \right]^2 \tag{6}$$

$$RMSE = \sqrt{\frac{1}{n} \sum_{i=1}^{n} (x_i - y_i)^2} \quad (\mathrm{mm}) \tag{7}$$

$$MAE = \left(\left| \frac{x_i - y_i}{n} \right| \right) \ (\mathrm{mm}) \tag{8}$$

$$Bias = \frac{\sum_{i=1}^{n} (x_i - y_i)}{n} \quad (\mathrm{mm}) \tag{9}$$

where x_i and $\overline{x}$ are the satellite values and their average and y_i and $\overline{y}$ are the observed values and their average by the models.

In this study, an optimized ANN model was used to predict precipitation using GA, PSO, and ICA algorithms.

3. Results and Discussion

Using PSO, ICA, and GA optimized models, an ANN-based downscaling method was formed. A statistical relationship between precipitation and CWP, COT, CER, and temperature at a coarse IMERG resolution was established using nonlinear regression analysis. To implement this, the auxiliary variables (with fine spatial resolution) were remapped via the bilinear method to a 0.1° resolution. The downscaling method assumed that the statistical relationship among the IMERG precipitation data and the auxiliary data at coarse spatial scale (0.1° × 0.1°) was equally valid at a finer, 1 km × 1 km scale. Moreover, a sensitivity analysis conducted determined how independent (auxiliary) variables as inputs would impact a model's output (dependent variable). The sensitivity analysis enabled us to identify the strengths and weaknesses of different input variables with respect to the sensitivity of precipitation observation.

At first, the predicted models were examined against the IMERG product to determine which model could estimate precipitation according to its target data (IMERG). Afterward, the results were validated through 54 in situ observations distributed over five 2015 heavy precipitation events. In addition to ANN's results, the results of the optimized ANN models (e.g., ICA, GA, and PSO), to assess the impact of optimization algorithms, were also validated.

The validation of the different predicted models (based on the desired precipitation estimation, IMERG) demonstrated various accuracies. The results for each individual event and the average of all events with respect to each model are presented in Table 6.

3.1. Precipitation Prediction Using ANN

The characteristics of the ANN model used in this study can be seen in Table 2. According to the ANN model, the predicted precipitation of the five precipitation events in Northeast Austria were calculated (Figure 4). Increasing the number of layers may help to reduce the error, and consequently, more accurate results could be obtained. According to Table 6, the statistical indices of the ANN model revealed the best performance on 17 April 2015 in terms of RMSE, MAE, and bias, while the lowest accuracy was obtained on 03 September 2015. The statistical indices for the best performance indicated RMSE = 5.84 mm, MAE = 6.21 mm, R^2 = 0.65, and bias = 0.01 mm, while results on 03 September 2015 showed RMSE = 6.13 mm, MAE = 8.01 mm, R^2 = 0.49, and bias = 0.52 mm.

Table 2. Characteristics of the artificial neural network (ANN).

	Structure	Train Function	Functions
Parameter	*25 20 output*	*LM*	*Tansig purelin*

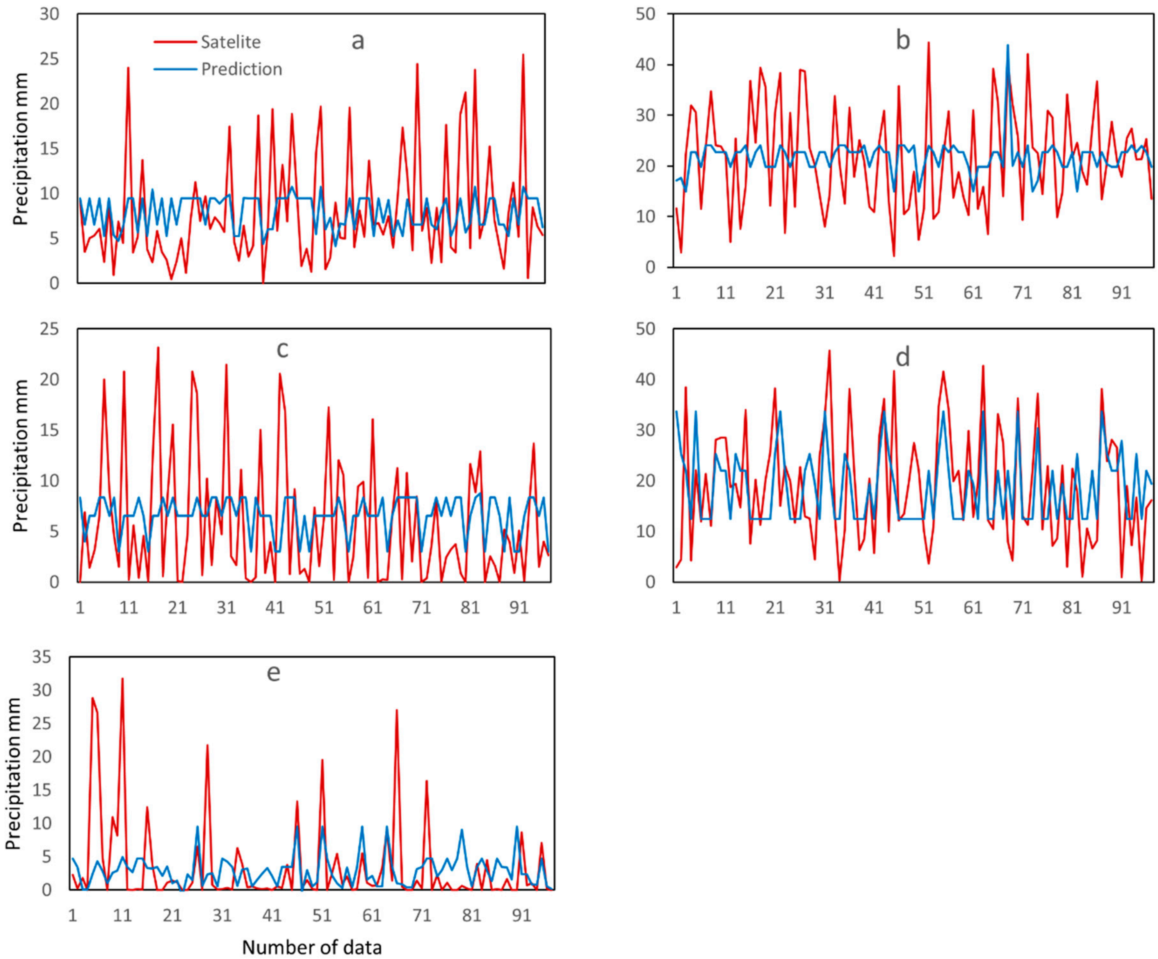

Figure 4. ANN predicted precipitation of the five events over Northeast Austria for (**a**) 17 April, (**b**) 23 May, (**c**) 3 September, (**d**) 25 September, and (**e**) 7 October 2015.

3.2. Precipitation Prediction Using Optimized ANN-based GA

The characteristics of the optimized ANN-based GA algorithm can be seen in Table 3. Moreover, according to GA, the predicted precipitation of the five precipitation events in Northeast Austria were calculated (Figure 5.). Increasing the number of iterations may help to reduce error and consequently, more accurate results could be obtained (see Table 3).

Table 3. Characteristics of the optimized ANN-based genetic algorithm (GA).

	Population	Crossover Rate	Mutation Rate	Number of Irritation	Structure
Parameter	*50*	*0.7*	*0.1*	*1000*	25–20 output

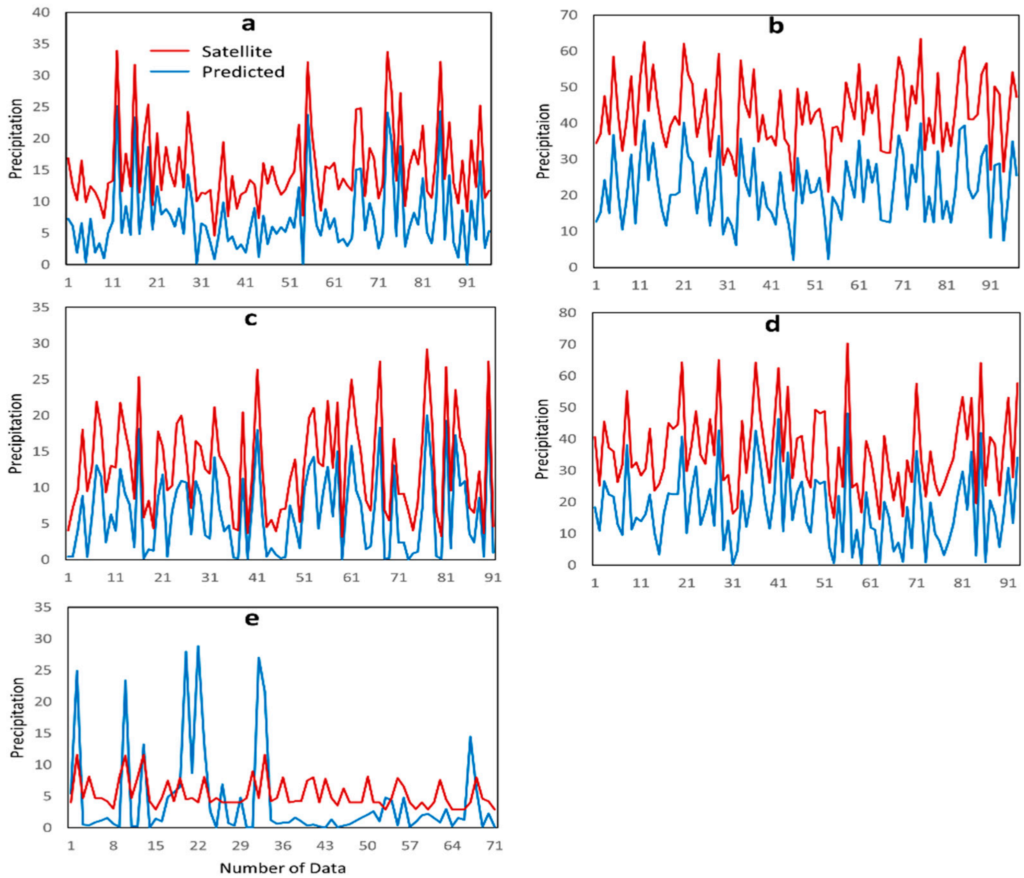

Figure 5. GA predicted precipitation of the five events over Northeast Austria for (**a**) 17 April 2015, (**b**) 23 May 2015, (**c**) 3 September 2015, (**d**) 25 September 2015, and (**e**) 7 October 2015.

The statistical analysis of the optimized ANN-based GA algorithm showed the highest and lowest models' accuracy on the days 17 April 2015 and 25 September 2015, respectively. Accordingly, the statistical indices indicated the RMSE = 4.96 mm, MAE = 8.61 mm, R^2 = 0.67, bias = −1.27 mm on 17 April 2015, while on 25 September 2015 the results revealed the RMSE = 11.32 mm, MAE = 8.06 mm, R^2 = 0.71, bias = 0.88 mm. Statistical indices indicated acceptable accuracy for prediction data. The significant difference between the original IMERG and the model prediction in Figure 5e compare to the Figure 5a–d, was probably due to the less correlation between input and output data.

Moreover, in all algorithms, to eliminate NaN (Not a Number) data, the input and output data that had zero values were eliminated. To have less NaN data, the original temperature unit of ERA5 (Kelvin) was used.

3.3. Precipitation Prediction Using Optimized ANN-based PSO

To optimize the ANN in accordance with the PSO algorithm, the following characteristics were chosen for this model. Increasing the iteration may reduce the error value in the test stage, and consequently, more accurate results may be obtained when repetition is increased. Moreover, the optimal structure of this algorithm was obtained after changing in swarm size, max iteration, and number and type of neurons function (Table 4).

Table 4. Characteristics and parameters of the optimized ANN-based particle swarm optimization (PSO).

	Swarm Size	Max Iteration	Structure
Parameter	300	60	25–20 output

Per the statistical analysis for the optimized ANN-based PSO in Table 6 and Figure 6, the best and least robust performances of the algorithm were on 03 September 2015 and 25 September 2015. The statistical analyses for 25 September 2015 and 03 September 2015 were RMSE = 11.41 mm, MAE = 6.08 mm, R^2 = 0.75, bias = -0.32 mm and RMSE = 5.3 mm, MAE = 6.09 mm, R^2 = 0.6, bias = 0.58 mm, respectively.

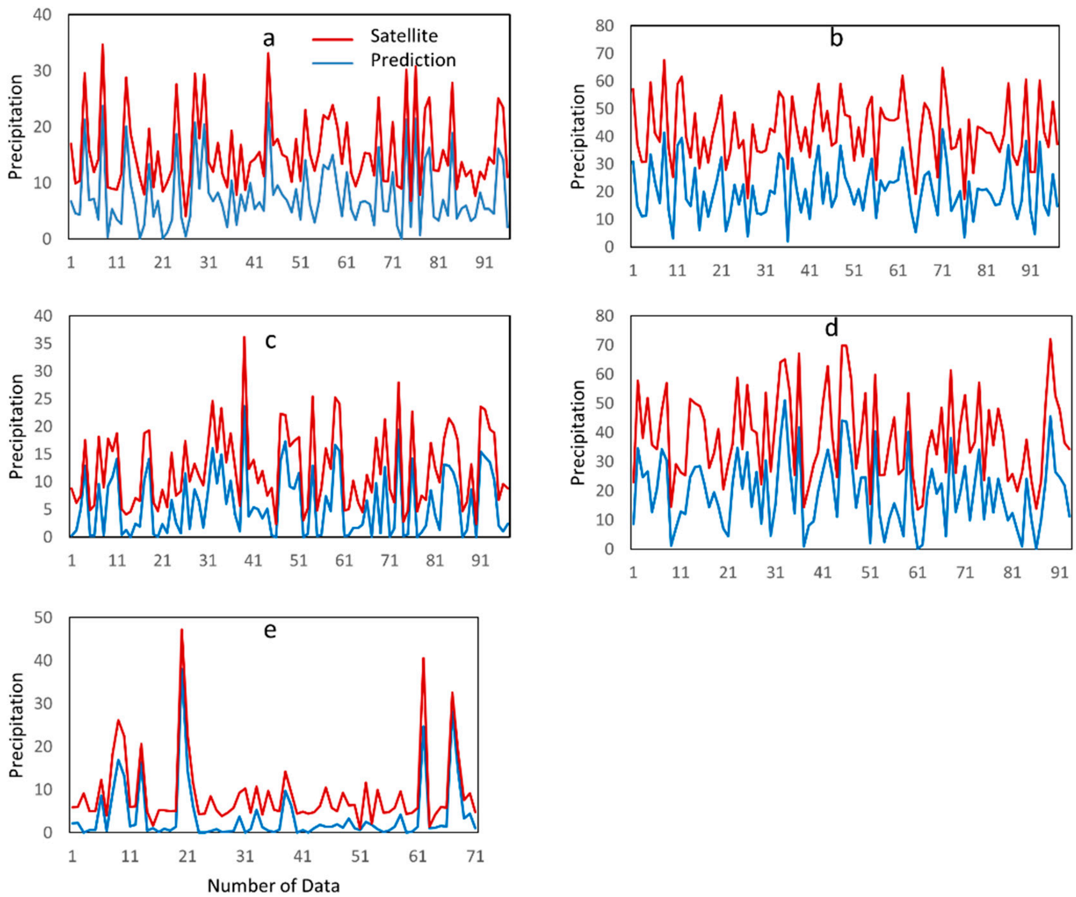

Figure 6. PSO predicted precipitation of the five events over Northeast Austria for (**a**) 17 April 2015, (**b**) 23 May 2015, (**c**) 03 September 2015, (**d**) 25 September 2015, and (**e**) 07 October 2015.

3.4. Precipitation Prediction Using Optimized ANN-based ICA

To optimize the ANN in accordance with the ICA algorithm, the following optimal network structure for this dataset was chosen. As shown in Table 5, there was a straight relation between number of countries, imperialisms, and decades, so increasing the number of decades, which means more repetition in the network, can conclude more accurate results.

Table 5. Parameters of each imperialist competitive algorithm (ICA).

	Number of Country	Number of Imperialism	Number of Decades	Revolution
Parameter	150	10	50	0.1

Following the ANN-based ICA algorithm, the aforementioned five precipitation events were predicted as well (Table 5 and Figure 7).

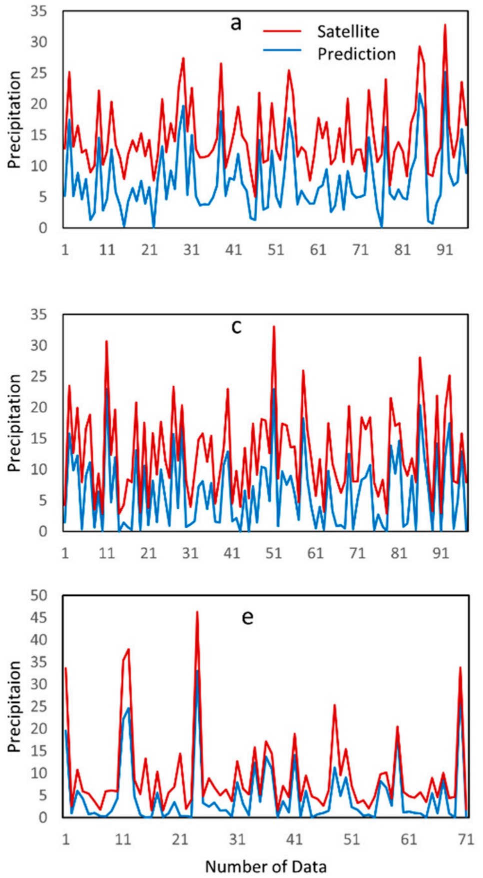

Figure 7. ICA predicted precipitation of the five events over Northeast Austria for (**a**) 17 April 2015, (**b**) 23 May 2015, (**c**) 3 September 2015, (**d**) 25 September 2015, and (**e**) 7 October 2015.

In addition, the ANN-based ICA algorithm was tested to predict the aforementioned five heavy precipitation events. According to Table 6 and Figure 7 the statistical values showed the values of RMSE = 5.26 mm, MAE = 6.06 mm, R^2 = 0.67, bias = 0.07 mm for 17 April 2015 and RMSE = 10.74 mm, MAE = 5.8 mm, R^2= 0.75, bias = −0.06 mm for 25 September 2015 as the best and worst predicted days, respectively. Table 6 shows the performance comparison among the ANN and the three optimized ANN algorithms for precipitation prediction. Overall, the performance of ANN-based ICA yielded better results than other algorithms according to these datasets.

Rain gauge observations were compared against by the original IMERG data and all the approaches of downscaling. The ANN, PSO, ICA, and GA models' results are presented in Table 7 and Figure 8 (as an example for 23 May 2015). The visualization comparison of the models shows significantly similar spatial distribution patterns compared to that of the original IMERG. According to the validation results, the residual correction technique improved the final downscaled results significantly. Table 7 presents the averaged results as well, and shows that all models can improve the CC, RMSE, and MAE effectively after residual correction. It indicates that after the residual correction, all models can effectively improve the CC, RMSE, and MAE, as shown by the average results of all events. It should be mentioned that parts of the precipitation that cannot be solely explained by cloud variables are indicated by residual mapping (Refer to Sharifi et al. [19]).

Table 6. Performance of the models using statistical indices-based evaluations for five heavy daily precipitation events over Northeast Austria.

Method	Index	Days					
		17 April 2015	**23 May 2015**	**03 September 2015**	**25 September 2015**	**07 October 2015**	**Average**
ANN	RMSE	5.84	9.69	6.13	11.81	6.52	8
ANN-GA		4.96	8.75	5.4	11.32	6.82	7.45
ANN-PSO		5.62	8.85	5.3	11.41	6.44	7.52
ANN-ICA		5.26	8.4	5.69	10.74	6.19	**7.3**
ANN	MAE	6.21	6.22	8.01	6.98	6.21	6.726
ANN-GA		8.61	8.81	7.73	8.06	6.48	7.9
ANN-PSO		6.06	6.09	6.09	6.08	4.95	**5.8**
ANN-ICA		6.06	6.21	6.21	5.8	4.95	**5.8**
ANN	R^2	0.65	0.69	0.49	0.7	0.25	0.56
ANN-GA		0.67	0.86	0.62	0.71	0.35	0.64
ANN-PSO		0.67	0.67	0.6	0.75	0.36	0.61
ANN-ICA		0.67	0.86	0.56	0.75	0.48	0.67
ANN	Bias	−0.01	0.03	0.52	−0.1	−0.27	0.17
ANN-GA		−1.27	0.91	0.21	0.88	−1.06	**−0.07**
ANN-PSO		−0.08	1.4	0.58	−0.32	1.18	0.55
ANN-ICA		0.07	−0.75	−0.1	−0.06	0.46	**−0.07**

Table 7. Evaluation statistics for all final downscaled products for the selected events over Northeast Austria.

Methods	Index	Days					
		17 April 2015	**23 May 2015**	**03 September 2015**	**25 September 2015**	**07 October 2015**	**Average**
IMERG	Bias (mm)	2.27	−10.84	−8.98	9.85	−1.29	**−1.80**
ANN_{final}		1.77	−7.92	−4.45	−0.27	−7.86	−3.75
PSO_{final}		1.74	−7.66	−4.44	−0.26	−7.84	−3.69
GA_{final}		1.70	−7.78	0.92	−0.28	−7.60	−2.61
ICA_{final}		1.74	−7.66	−4.44	−0.26	−7.84	−3.69
ANN		0.59	−12.20	−2.39	0.82	1.60	−2.32
ANN_{PSO}		−0.43	−10.42	−5.54	4.68	−5.22	−3.39
ANN_{GA}		−0.29	−10.85	−5.23	4.74	−3.51	−3.03
ANN_{ICA}		−1.59	−10.58	−5.70	4.87	−5.54	−3.71
IMERG	CC	0.65	0.51	0.25	0.16	-0.07	0.30
ANN_{final}		0.66	0.43	0.73	0.75	0.22	0.56
PSO_{final}		0.69	0.42	0.74	0.76	0.23	**0.57**
GA_{final}		0.69	0.44	−0.69	0.76	0.39	0.32
ICA_{final}		0.69	0.44	0.74	0.76	0.23	**0.57**
ANN		0.14	0.19	0.30	0.15	−0.04	0.15
ANN_{PSO}		0.08	−0.04	−0.32	−0.40	0.15	−0.11
ANN_{GA}		0.42	0.10	0.14	−0.07	−0.12	0.09
ANN_{ICA}		0.29	0.06	−0.41	−0.33	0.17	−0.04
IMERG	MAE (mm)	4.26	12.58	9.86	13.07	10.96	10.14
ANN_{final}		3.93	11.06	5.45	4.78	7.87	6.62
PSO_{final}		3.75	10.56	5.35	4.79	7.86	**6.46**
GA_{final}		3.75	10.56	13.81	4.79	7.69	8.12
ICA_{final}		3.75	10.56	5.35	4.79	7.86	**6.46**
ANN		5.28	13.07	7.26	14.41	10.29	10.06
ANN_{PSO}		3.84	11.32	8.99	12.01	6.01	8.43
ANN_{GA}		3.45	11.86	8.44	10.28	7.03	8.21
ANN_{ICA}		3.70	11.31	9.02	10.47	6.27	8.15

Table 7. *Cont.*

Methods	Index	Days					
		17 April 2015	23 May 2015	03 September 2015	25 September 2015	07 October 2015	Average
IMERG	RMSE (mm)	6.28	15.15	12.97	17.37	15.76	13.50
ANN_{final}		5.39	13.53	7.84	7.10	10.31	8.84
PSO_{final}		5.33	12.64	7.77	7.10	10.31	**8.63**
GA_{final}		5.33	12.64	15.67	7.10	9.88	10.12
ICA_{final}		5.33	12.64	7.77	7.10	10.31	**8.63**
ANN		7.12	15.91	9.45	20.37	12.45	13.06
ANN_{PSO}		5.32	14.57	11.63	14.53	8.59	10.93
ANN_{GA}		4.81	14.82	10.85	12.79	10.61	10.77
ANN_{ICA}		5.30	14.57	11.77	12.85	8.76	10.65

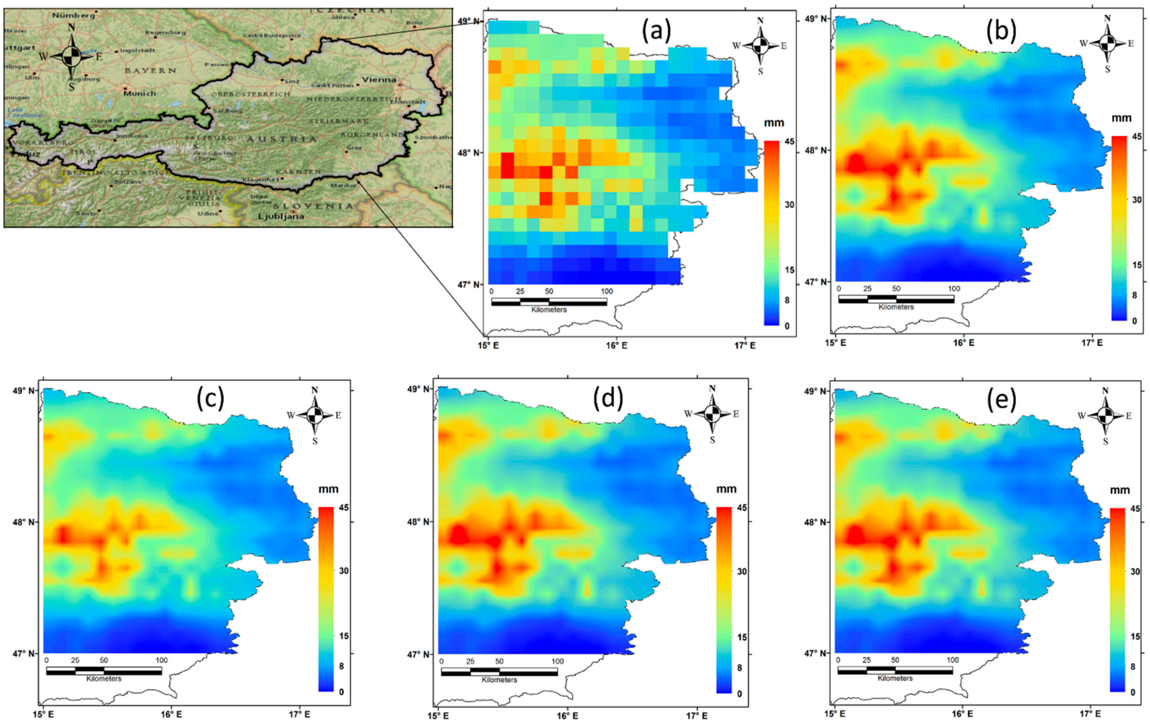

Figure 8. (**a**) Original Integrated Multi-satellite Retrievals for GPM; Global Precipitation Measurement (IMERG) and the final downscaled products through (**b**) ANN, (**c**) GA, (**d**) ICA, (**e**) PSO for 23 May 2015 event over Northeast Austria.

The residual technique was also employed in this study after the precipitation downscaling for all models, since the models themselves may not properly explain precipitation variability to the fullest extent [22,29].

Although residual correction results from downscaling methods came close, observed differences were present among events (hereafter when residual correction is employed they will call *final*). The estimation of bias, CC, MAE, and RMSE was conducted by different models and an average is given for all events and the results can be seen in Table 7. On average, ANN_{final} and the original IMERG indicated the highest and lowest bias (−3.75 mm and −1.80 mm, respectively), while PSO_{final} and ICA_{final} yielded the highest CC (0.57), lowest MAE (6.46 mm), and RMSE (8.63 mm). It should be mentioned that downscaled results derived from the POS and ICA after residual correction showed similar results. As can be seen, with respect to bias, all models indicated underestimation of precipitation with the negative bias values. The underestimation of precipitation might be due to the reliability and availability of the data. The cloud optical and microphysical images are available 1–2 time daily, therefore the possibility of precipitation occurrence before or after satellite passage time over the study area may lead to underestimation of precipitation by the models. Another cause might be the availability of the MODIS cloud variables only for daytime. Moreover, overestimation or underestimation of the satellite data could be due to some other reasons, such as: (i) The spatial resolution of the satellite product, since precipitation within a region may occur on smaller scales than the pixel size of satellites; (ii) short-time precipitation is much more variable than daily precipitation, for example; (iii) systematic error; (iv) difficulties to capture precipitation over complex terrain, etc.

3.5. Sensitivity Analysis

Sensitivity analysis determines how independent variables (inputs) will impact a model's output (dependent variable). This technique is used within specific boundaries that depend on one or more input variables [43]. In this study, according to statistical analysis, the optimized ANN-based ICA was selected as the best network and then sensitivity analysis on this network was performed. For the sensitivity analysis, the four parameters used in our models as input to predict the precipitation (COT, CER, CWP, temperature) were extracted individually and then the errors resulting from the elimination of each parameter were obtained. Afterward, the most influential input parameter was obtained.

Table 8 and Figure 9 show the effectiveness of all input variables for each individual event. One can find that the most effective and ineffective parameters in predicting precipitation in this study were COT and temperature, respectively. However, all four parameters had the same degree of importance in predicting precipitation on 07 October 2015, 23 May 2015, and 25 September 2015.

Table 8. Statistical indices after sensitivity analysis of daily precipitation estimates.

DAYS	ERROR	Without CER	Without COT	Without CWP	Without TEM
03 September 2015	RMSE	5.86	5.45	6.46	5.92
	MAE	6.21	6.21	6.21	6.21
	R^2	0.49	0.61	0.55	0.55
07 October 2015	RMSE	6.9	7.54	6.95	4.89
	MAE	8.36	8.36	8.36	8.36
	R^2	0.33	0.13	0.24	0.48
17 April 2015	RMSE	5.64	5.7	5.86	5.45
	MAE	6.06	6.06	6.06	6.06
	R^2	0.65	0.64	0.67	0.64
23 May 2015	RMSE	9.39	11.01	9.82	10.14
	MAE	6.04	6.04	6.04	6.04
	R^2	0.86	0.81	0.83	0.83
25 September 2015	RMSE	12.39	13.32	13.25	11.79
	MAE	6.08	6.08	6.08	6.08
	R^2	0.72	0.7	0.64	0.77

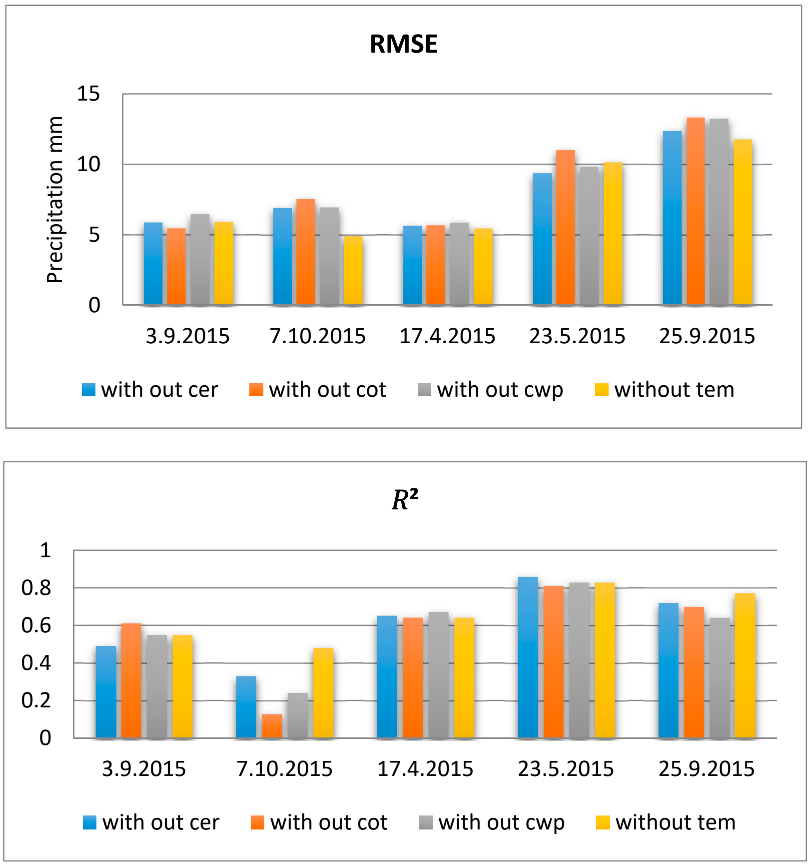

Figure 9. Sensitivity analysis of error calculation for a) RMSE and b) R-squared (R^2)

4. Conclusions

This study explored the applicability of the downscaling technique using the optimized ANN to produce daily precipitation data with more details over Northeast Austria and compared the results with simple ANN method.

The satellite precipitation data as output and the four parameters COT, CWP, CET, and temperature as inputs were introduced to the network. In order to improve the performance of ANN, optimized ANN algorithms such as PSO, ICA, and GA were used. In all algorithms, to eliminate NaN data, the input and output data which had zero values were removed. To have less NaN data, the ERA5's original temperature unit (Kelvin) was used and temperatures were not converted to Celsius. Moreover, to assess the network performance, the statistical indices, RMSE, R^2, MAE, and bias were used. The study results demonstrated that use of optimized ANN-based models were successful and increased the accuracy of the predicted heavy daily precipitation data in comparison to using only the ANN method.

According to the validation results of the optimized ANN, the best performance of ICA was on 17 May 2015 (RMSE = 5.26 mm, MAE = 6.06 mm, R2 = 0.67, bias = 0.07 mm) with error indices (RMSE = 5.26 mm, MAE = 6.06 mm, R^2 = 0.67, bias = 0.07 mm), and the worst performance was on 25 September 2015. According to the GA's results, its best performance was on 17 April 2015 and the worst performance occurred on 25 September 2015. Finally, the best and worst performances for the PSO were on 03 September 2015 and 25 September 2015, respectively. These have been calculated according to the predicted precipitation estimation against the original IMERG as the desired target data.

Moreover, the sensitivity analysis of the network's inputs was conducted and individual input parameters were eliminated, according to the best-optimized network algorithm (ICA). Overall all four parameters did not have a significant difference, however, it should be mentioned that according to sensitivity analysis, the results showed that COT was the most effective parameter used in this study to predict precipitation. On 07 October 2015, 23 May 2015, and 25 September 2015 the most effective parameter was COT and overall temperature and CWP indicated the least effects. The accuracy of the final downscaled satellite precipitation notably enhanced after implementation of the residual correction algorithms. ICA slightly outperformed other algorithms when compared to the other optimized ANN algorithms used to downscale the IMERG product. There is a chance that precipitation occured in periods between satellite pass by the study area and this could have caused some errors in establishing relationships. Since cloud optical properties, as well as microphysical properties, are solely available during the day, this could be an added cause for this type of error.

The proposed methodology optimizes the widely used ANN for downscaling aims. One of the main contributions of our study was to optimize the ANN downscaling methodology and incorporate freely distributed satellite MODIS and ERA5 data in the downscaling process. The application of global scale auxiliary (input) data into other geographical regions as well as other applications is another great advantage. While easily adaptable to other geographical locations, it is recommended that further advanced experimentation with a variety of architectures is conducted, using optimized ANN models for data selection and input combinations.

Further studies could also explore a comparison of various downscaling techniques, in particular, machine learning methodology, with more attention to data outliers and time series evaluation of these methods. The downscaling process and the exclusive use of MODIS and recently released ERA5 data offers the possibility to use fine-resolution, freely distributed satellite data for downscaling.

Author Contributions: Conceptualization: A.H.S., J.M.S., and E.S.; methodology: A.H.S., E.S. and M.R.H.; software: A.H.S.; validation, E.S.; formal analysis, A.H.S.; investigation, A.H.S., J.M.S. and E.S.; data curation, E.S.; writing—original draft preparation, A.H.S., M.R.H., A.N., J.M.S. and E.S; writing—review and editing, A.H.S., M.R.H., A.N., J.M.S., H.v.R. and E.S.; visualization, E.S. and A.H.S.; supervision, J.M.S. and E.S.

Funding: This research received no external funding.

Acknowledgments: NASA/Goddard Space Flight Center's and PPS provided the IMERG data. These data drive the development and computations of IMERG as a contribution to GPM constellation satellites which is then archived at the NASA GES DISC (https://disc.sci.gsfc.nasa.gov/SSW; accessed on 26 August 2017). The MODIS datasets are available from the Atmosphere Archive and Distribution System (LAADS) web interface (https://ladsweb.modaps.eosdis.nasa.gov/search/imageViewer/42/MOD06_L2--6; accessed on 26 November 2017). In situ data from meteorological synoptic stations were provided by the Zentralanstalt für Meteorologie und Geodynamik (ZAMG)-Austria. We acknowledge the ECMWF-ERA5 datasets from the Climate Data Store (CDS) of the European Centre for Medium Range Weather Forecasts, accessed on January 2019, available from https://cds.climate.copernicus.eu/cdsapp#!/home. The Open Access publishing was supported by the University of Vienna Open Access Publishing Fund.

Conflicts of Interest: The authors declare no conflict of interest.

References

1. Prasanna, V.; Subere, J.; Das, D.K.; Govindarajan, S.; Yasunari, T. Development of daily gridded rainfall dataset over the Ganga, Brahmaputra and Meghna river basins. *Met. Apps* **2014**, *21*, 278–293. [CrossRef]
2. Gampe, D.; Ludwig, R. Evaluation of Gridded Precipitation Data Products for Hydrological Applications in Complex Topography. *Hydrology* **2017**, *4*, 53. [CrossRef]
3. Tseng, K.-H.; Shum, C.K.; Lee, H.; Duan, J.; Kuo, C.; Song, S.; Zhu, W. Satellite Observed Environmental Changes over the Qinghai-Tibetan Plateau. *Terr. Atmos. Ocean. Sci.* **2011**, *22*, 229–239. [CrossRef]
4. Chen, D.; Tian, Y.; Yao, T.; Ou, T. Satellite measurements reveal strong anisotropy in spatial coherence of climate variations over the Tibet Plateau. *Sci. Rep.* **2016**, *6*, 30304. [CrossRef] [PubMed]
5. Beck, H.E.; Pan, M.; Roy, T.; Weedon, G.P.; Pappenberger, F.; van Dijk, A.I.J.M.; Huffman, G.J.; Adler, R.F.; Wood, E.F. Daily evaluation of 26 precipitation datasets using Stage-IV gauge-radar data for the CONUS. *Hydrol. Earth Syst. Sci.* **2019**, *23*, 207–224. [CrossRef]
6. Karger, D.N.; Conrad, O.; Böhner, J.; Kawohl, T.; Kreft, H.; Soria-Auza, R.W.; Zimmermann, N.E.; Linder, H.P.; Kessler, M. Climatologies at high resolution for the earth's land surface areas. *Sci. Data* **2017**, *4*, 170122. [CrossRef]
7. Prakash, S. Performance assessment of CHIRPS, MSWEP, SM2RAIN-CCI, and TMPA precipitation products across India. *J. Hydrol.* **2019**. [CrossRef]

8. Zhang, A.; Xiao, L.; Min, C.; Chen, S.; Kulie, M.; Huang, C.; Liang, Z. Evaluation of latest GPM-Era high-resolution satellite precipitation products during the May 2017 Guangdong extreme rainfall event. *Atmos. Res.* **2019**, *216*, 76–85. [CrossRef]
9. Sharifi, E.; Steinacker, R.; Saghafian, B. Assessment of GPM-IMERG and Other Precipitation Products against Gauge Data under Different Topographic and Climatic Conditions in Iran: Preliminary Results. *Remote Sens.* **2016**, *8*, 135. [CrossRef]
10. Huffman, G.; Bolvin, D.; Nelkin, E. Integrated Multi-satellitE Retrievals for GPM (IMERG) Technical Documentation. *NASA/GSFC Code* **2015**, *612*, 2019.
11. Huffman, G.J.; Bolvin, D.T.; Nelkin, E.J.; Wolff, D.B.; Adler, R.F.; Gu, G.; Hong, Y.; Bowman, K.P.; Stocker, E.F. The TRMM Multisatellite Precipitation Analysis (TMPA): Quasi-Global, Multiyear, Combined-Sensor Precipitation Estimates at Fine Scales. *J. Hydrometeorol.* **2007**, *8*, 38–55. [CrossRef]
12. Dee, D.P.; Uppala, S.M.; Simmons, A.J.; Berrisford, P.; Poli, P.; Kobayashi, S.; Andrae, U.; Balmaseda, M.A.; Balsamo, G.; Bauer, P.; et al. The ERA-Interim reanalysis: Configuration and performance of the data assimilation system. *Q. J. R. Meteorol. Soc.* **2011**, *137*, 553–597. [CrossRef]
13. Sharifi, E.; Steinacker, R.; Saghafian, B. Multi time-scale evaluation of high-resolution satellite-based precipitation products over northeast of Austria. *Atmos. Res.* **2018**, *206*, 46–63. [CrossRef]
14. Tao, K.; Barros, A.P. Using Fractal Downscaling of Satellite Precipitation Products for Hydrometeorological Applications. *J. Atmos. Ocean. Technol.* **2010**, *27*, 409–427. [CrossRef]
15. Sharifi, E.; Steinacker, R.; Saghafian, B. Hourly Comparison of GPM-IMERG-Final-Run and IMERG-Real-Time (V-03) over a Dense Surface Network in Northeastern Austria. In Proceedings of the European Geosciences Union General Assembly, Vienna, Austria, 23–28 April 2017.
16. Sharifi, E.; Saghafian, B.; Steinacker, R. Copula-based Stochastic Uncertainty Analysis of Satellite Precipitation Products. *J. Hydrol.* **2019**. [CrossRef]
17. Coulibaly, P.; Dibike, Y.B.; Anctil, F. Downscaling Precipitation and Temperature with Temporal Neural Networks. *J. Hydrometeorol.* **2005**, *6*, 483–496. [CrossRef]
18. Salimi, A.; Karami, H.; Farzin, S.; Hassanvand, M.; Azad, A.; Kisi, O. Design of water supply system from rivers using artificial intelligence to model water hammer. *ISH J. Hydraul. Eng.* **2019**, *20*, 1–10. [CrossRef]
19. Hassanvand, M.R.; Karami, H.; Mousavi, S.-F. Investigation of neural network and fuzzy inference neural network and their optimization using meta-algorithms in river flood routing. *Nat. Hazards* **2018**, *94*, 1057–1080. [CrossRef]
20. Khan, K.; Sahai, A. A Comparison of BA, GA, PSO, BP and LM for Training Feed forward Neural Networks in e-Learning Context. *IJISA* **2012**, *4*, 23–29. [CrossRef]
21. Such, F.P.; Madhavan, V.; Conti, E.; Lehman, J.; Stanley, K.O.; Clune, J. Deep Neuroevolution: Genetic Algorithms Are a Competitive Alternative for Training Deep Neural Networks for Reinforcement Learning. *arXiv* **2017**, arXiv:1712.06567v3.
22. Sharifi, E.; Saghafian, B.; Steinacker, R. Downscaling Satellite Precipitation Estimates With Multiple Linear Regression, Artificial Neural Networks, and Spline Interpolation Techniques. *J. Geophys. Res. Atmos.* **2019**, *75*, 606. [CrossRef]
23. Immerzeel, W.W.; Rutten, M.M.; Droogers, P. Spatial downscaling of TRMM precipitation using vegetative response on the Iberian Peninsula. *Remote Sens. Environ.* **2009**, *113*, 362–370. [CrossRef]
24. Platnick, S.; Meyer, K.G.; King, M.D.; Wind, G.; Amarasinghe, N.; Marchant, B.; Arnold, G.T.; Zhang, Z.; Hubanks, P.A.; Holz, R.E.; et al. The MODIS cloud optical and microphysical products: Collection 6 updates and examples from Terra and Aqua. *IEEE Trans. Geosci. Remote Sens.* **2017**, *55*, 502–525. [CrossRef]
25. Retalis, A.; Tymvios, F.; Katsanos, D.; Michaelides, S. Downscaling CHIRPS precipitation data: An artificial neural network modelling approach. *Int. J. Remote Sens.* **2017**, *38*, 3943–3959. [CrossRef]
26. Copernicus Climate Change Service (C3S). Fifth Generation of ECMWF Atmospheric Reanalyses of the Global Climate; Copernicus Climate Change Service. 2017. Available online: https://cds.climate.copernicus.eu/cdsapp#!/home (accessed on 10 August 2019).
27. Rubel, F.; Brugger, K.; Haslinger, K.; Auer, I. The climate of the European Alps: Shift of very high resolution Köppen-Geiger climate zones 1800–2100. *Metz* **2017**, *26*, 115–125. [CrossRef]

28. Platnick, S.; King, M.D.; Meyer, K.G.; Wind, G.; Amarasinghe, N.; Marchant, B.; Arnold, G.T.; Zhang, Z.; Hubanks, P.; Ridgway, B.; et al. MODIS Cloud Optical Properties: User Guide for the Collection 6 Level-2 MOD06/MYD06 Product and Associated Level-3 Datasets. 2015. Available online: https://modis-images.gsfc.nasa.gov/_docs/C6MOD06OPUserGuide.pdf (accessed on 10 August 2019).
29. Alexakis, D.D.; Tsanis, I.K. Comparison of multiple linear regression and artificial neural network models for downscaling TRMM precipitation products using MODIS data. *Environ. Earth Sci.* **2016**, *75*, 606. [CrossRef]
30. Park, N.-W. Spatial Downscaling of TRMM Precipitation Using Geostatistics and Fine Scale Environmental Variables. *Adv. Meteorol.* **2013**, *2013*, 1–9. [CrossRef]
31. Xu, G.; Xu, X.; Liu, M.; Sun, A.; Wang, K. Spatial Downscaling of TRMM Precipitation Product Using a Combined Multifractal and Regression Approach: Demonstration for South China. *Water* **2015**, *7*, 3083–3102. [CrossRef]
32. He, X.; Chaney, N.W.; Schleiss, M.; Sheffield, J. Spatial downscaling of precipitation using adaptable random forests. *Water Resour. Res.* **2016**, *52*, 8217–8237. [CrossRef]
33. Darji, M.P.; Dabhi, V.K.; Prajapati, H.B. Rainfall forecasting using neural network: A survey. In Proceedings of the 2015 International Conference on Advances in Computer Engineering and Applications (ICACEA), Ghaziabad, India, 19–20 March 2015; pp. 706–713, ISBN 978-1-4673-6911-4.
34. Coulibaly, P.; Anctil, F.; Bobée, B. Daily reservoir inflow forecasting using artificial neural networks with stopped training approach. *J. Hydrol.* **2000**, *230*, 244–257. [CrossRef]
35. Bishop, C.M. *Neural Networks for Pattern Recognition*; Clarendon Press: Oxford, UK, 1995; ISBN 0198538642.
36. Atashpaz-Gargari, E.; Lucas, C. Imperialist competitive algorithm: An algorithm for optimization inspired by imperialistic competition. In Proceedings of the 2007 IEEE Congress on Evolutionary Computation, Singapore, 25–28 September 2007; pp. 4661–4667, ISBN 978-1-4244-1339-3.
37. Shamshirband, S.; Gocić, M.; Petković, D.; Javidnia, H.; Ab Hamid, S.H.; Mansor, Z.; Qasem, S.N. Clustering project management for drought regions determination: A case study in Serbia. *Agric. For. Meteorol.* **2015**, *200*, 57–65. [CrossRef]
38. McCall, J. Genetic algorithms for modelling and optimisation. *J. Comput. Appl. Math.* **2005**, *184*, 205–222. [CrossRef]
39. Krohling, R.A.; Rey, J.P. Design of optimal disturbance rejection PID controllers using genetic algorithms. *IEEE Trans. Evol. Comput.* **2001**, *5*, 78–82. [CrossRef]
40. Wan, W.; Birch, J.B. An Improved Hybrid Genetic Algorithm with a New Local Search Procedure. *J. Appl. Math.* **2013**, *2013*, 1–10. [CrossRef]
41. Sette, S.; Boullart, L. Genetic programming: Principles and applications. *Eng. Appl. Artif. Intell.* **2001**, *14*, 727–736. [CrossRef]
42. Kennedy, J.; Eberhart, R. Particle swarm optimization. In Proceedings of the ICNN'95-International Conference on Neural Networks, Perth, WA, Australia, 27 November–1 December 1995; pp. 1942–1948, ISBN 0-7803-2768-3.
43. Hassanvand, M.R.; Karami, H.; Mousavi, S.-F. Use of multi-criteria decision-making for selecting spillway type and optimizing dimensions by applying the harmony search algorithm: Qeshlagh Dam Case Study. *Lakes Reserve* **2018**, *27*, 111. [CrossRef]